Turkish Journal of Agriculture and Forestry

Volume 48 | Number 1 Article 4

2-1-2024

The flow field simulation and suction structure optimal design of the dual-airway pneumatic fallen jujube fruit pickup device

HUIZHE DING
dinghz@stu.shzu.edu.cn

JINGBIN LI
lijingbin@shzu.edu.cn

HUTING WANG
xgb@shzu.edu.cn

JING NIE
niejing19@shzu.edu.cn

LONGPENG DING
dy2016@shzu.edu.cn

See next page for additional authors

Recommended Citation

DING, HUIZHE; LI, JINGBIN; WANG, HUTING; NIE, JING; DING, LONGPENG; and KIRMIZIBİBER, ABDULLAH (2024) "The flow field simulation and suction structure optimal design of the dual-airway pneumatic fallen jujube fruit pickup device," *Turkish Journal of Agriculture and Forestry*: Vol. 48: No. 1, Article 4.
https://doi.org/10.55730/1300-011X.3160
Available at: https://journals.tubitak.gov.tr/agriculture/vol48/iss1/4

The flow field simulation and suction structure optimal design of the dual-airway pneumatic fallen jujube fruit pickup device

Authors
HUIZHE DING, JINGBIN LI, HUTING WANG, JING NIE, LONGPENG DING, and ABDULLAH KIRMIZIBİBER

Turkish Journal of Agriculture and Forestry

http://journals.tubitak.gov.tr/agriculture/

Research Article

Turk J Agric For
(2024) 48: 26-42

doi:10.55730/1300-011X.3160

Flow field simulation and suction structure optimal design of the dual-airway pneumatic fallen jujube fruit pickup device

Huizhe DING[1], Jingbin LI[1,2,*], Huting WANG[1,2], Jing NIE[1,2], Longpeng DING[1,2], Abdullah KIRMIZIBİBER[3]

[1]College of Mechanical and Electrical Engineering, Shihezi University, Shihezi, China
[2]Key Laboratory of Modern Agricultural Machinery of Xinjiang Production and Construction Corps, Shihezi, China
[3]City and Regional Planning, Faculty of Architecture and Design, Atatürk University, Erzurum, Turkiye

Received: 30.10.2023 • **Accepted/Published Online:** 25.12.2023 • **Final Version:** 01.02.2024

Abstract: To investigate the flow field characteristics within the cavity of the key components in a dual-airway pneumatic fallen jujube fruit pickup device under the influence of negative pressure airflow and to optimize the device's structural parameters, we constructed a numerical simulation model for the flow field in the dual-airway pickup mouth using computational fluid dynamics. Initially, we analyzed the impact of the central partition on the flow field within the pickup suction mouth.

Subsequently, utilizing the velocity unevenness coefficient as the response index, we conducted a single-factor test on the key parameters of the cavity structure to determine the optimal value range for each factor. Through an orthogonal test, response surface analysis, and a composite optimization method, we established the optimal structural parameter combination as follows: a falloff angle of 91.37°, an opening width of 50 mm, a flanging radius of 6.45 mm, and a relative height of 20mm, resulting in a velocity unevenness coefficient of 5.89%.

Finally, validation tests were performed, revealing that the velocity unevenness coefficients for dual-airway pickup suction were 6.22%, 6.60%, and 6.45%, respectively. The maximum deviation from the predicted value was 0.71%, with a maximum relative error of 12.05%. This study holds significant importance not only for the optimization of complex cavity structures in pickup equipment design but also serves as a valuable reference for the development of mechanized fallen jujube fruit pickup equipment.

Key words: Jujube equipment, CFD numerical simulation, dual-airway, pickup suction, optimized design

1. Introduction

Xinjiang stands out as the primary region for Chinese jujube production, consistently ranking first in jujube output throughout the year (Liu et al., 2021; Wang et al., 2022; Yan et al., 2022). Presently, dwarf dense planting represents the predominant cultivation method for red jujube. However, the mechanization of jujube harvest remains a critical challenge, impeding the sustainable growth of the jujube industry. This is primarily due to the impact of biological characteristics and external environmental factors (Li and Chao, 2022; Yang et al., 2022; Li and Ercisli, 2023). The falling rate of mature jujubes can reach 40% to 70% (He et al., 2023; Yang et al., 2023; Zhang et al., 2023), necessitating manual collection of fallen fruit. The high labor intensity, elevated labor costs, and the limited mechanization intelligence in jujube harvest significantly hinder the industry's healthy development (Ni et al., 2019; Zhou et al., 2020; Nie et al., 2022a, 2022b). Hence, there is an urgent need to develop jujube harvesting equipment with stable performance, which holds significant importance in accelerating the mechanization and enhancing the efficiency of jujube production, ultimately achieving cost reduction and increased efficiency in the jujube industry.

With the exception of India, Iran, South Korea, and a few other countries, China boasts the largest jujube planting area globally (Fu et al., 2018). While South Korean scholars abroad have explored related harvesting machinery (Li et al., 2022; Yang et al., 2023), the study of jujube harvesting equipment has been limited. In recent years, Chinese scholars have focused extensively on fallen jujube fruit pickup equipment (Shi et al., 2022; Zhou et al., 2022a, 2022b). The method of using negative pressure airflow for picking up fallen jujube fruit has proven effective in reducing damage, emerging as a current research hotspot in jujube harvesting machinery in Xinjiang (Li and Chao, 2022; Xu et al., 2022; Nie et al., 2023). However, the pneumatic fallen jujube fruit pickup equipment developed in China predominantly adopts a single air path

* Correspondence: lijingbin@shzu.edu.cn

arrangement (Fu et al., 2017), resulting in issues such as a narrow operation width, manual carrying or supporting straws during pickup, suboptimal continuous operation, and the inability to achieve full mechanized pickup.

Our team not only designed and developed the pneumatic fallen jujube fruit pickup equipment but also delved into its operating principles (Shi et al., 2022; Li and Chao, 2021). Building upon our team's research, this paper presents the design of a dual-airway pneumatic fallen jujube fruit pickup device equipped with the team's test prototype, enabling continuous operation without manual intervention. However, there remains a need to elucidate the flow field characteristics of its key components and optimize their structural parameters. Employing the computational fluid dynamics (CFD) method to study flow field characteristics offers advantages such as a short cycle and low cost, proving to be an effective means to acquire fluid parameters and flow field distribution (Blazek, 2015; Li and Ercisli, 2023).

We utilized the CFD method to simulate and analyze the flow field inside the air distribution chamber (Olatunde et al., 2016; Wang et al., 2019). Through orthogonal experimental design and numerical simulation, we determined the optimal structural parameters for achieving flow field uniformity in the air distribution chamber. Simultaneously, we explored the influence of various structural parameters and extended domain parameters of the dust suction device on the dust suction effect using a numerical simulation method (Ye et al., 2022). This allowed us to identify appropriate structural parameters to achieve an efficient cleaning effect. Some scholars optimized the design based on the analysis of the flow field characteristics of the structural parameters of the dust suction port (Li et al., 2016). Clearly, the numerical simulation method based on Fluent has become a crucial approach for studying cavity structure and optimizing structural parameters, with relevant technologies widely applied.

Given the uncertainties in the flow field characteristics of the designed dual-airway pneumatic fallen jujube fruit pickup device and the need for optimization of key component structural parameters, this paper aims to establish a numerical model of the flow field in the dual-airway pickup mouth. We intend to explore the flow field characteristics of the dual-airway pickup mouth under the influence of negative pressure airflow, and determine the main factors affecting the structure of the pickup mouth. Subsequently, we will conduct an orthogonal test to analyze the interaction of factors and, finally, carry out structural parameter optimization and experimental verification of the dual-airway pickup mouth body. This research is expected to contribute significantly to the advancement of pneumatic fallen jujube fruit pickup equipment. The primary contributions are outlined below:

(1) We designed a dual-airway pneumatic fallen jujube fruit pickup device, utilizing dual-airway pickup suction to increase the working width and achieve continuous operation without manual intervention.

(2) Through parameter optimization and experimental verification, our results indicate a substantial reduction in the velocity inhomogeneity of the dual-airway pickup mouth after optimization. The uniform distribution of air velocity at the inlet section of the suction mouth provides sufficient air velocity for jujube particle suspension.

2.Materials and methods

2.1. Device structure and working principle

2.1.1. Device structure

The experimental prototype (Shi et al., 2022) crafted by the team during the initial phase primarily comprises a transmission system, crawler-type walking chassis, conveying device, centrifugal fan, and cleaning separation device. The pickup device plays a pivotal role as a crucial component of the pneumatic conveying system for picking up red dates. This paper introduces the design of a dual-airway pneumatic fallen jujube fruit pickup device, featuring dual-airway pickup suction, a follow-up copying mechanism, suspension lifting parts, copying wheel, and other essential components. By incorporating an additional air path, this device is seamlessly integrated into the front end of the red date pickup prototype previously developed by our team. A visual representation of the test prototype and the device is depicted in Figure 1a.

2.1.2. Working principle

The pneumatic conveying system is comprised of a centrifugal fan, cleaning separation device, conveying hose, and pickup device. The operational principle of the device is illustrated in Figure 1b. During operation, the electric push rod lowers the dual-airway pickup suction, bringing it into contact with the ground. Simultaneously, the motor drives the centrifugal fan, generating negative pressure airflow for throughout the entire pneumatic conveying system. As the machine advances, red dates collected by the ground-mounted collection bar are progressively introduced into the mobile pickup suction body. In the anterior steering-flow area, horizontal negative pressure airflow accelerates the movement of the red dates, propelling them toward the suspension zone (located near the suction mouth). Some red dates assume a suspended state due to the vertical negative pressure airflow.

Conversely, a portion of the red dates, influenced by a weaker airflow, shifts to the posterior steering-flow area, where the gap between this area and the ground is smaller than the jujube grain size. These jujubes, after being affected by the reverse airflow in the posterior steering-

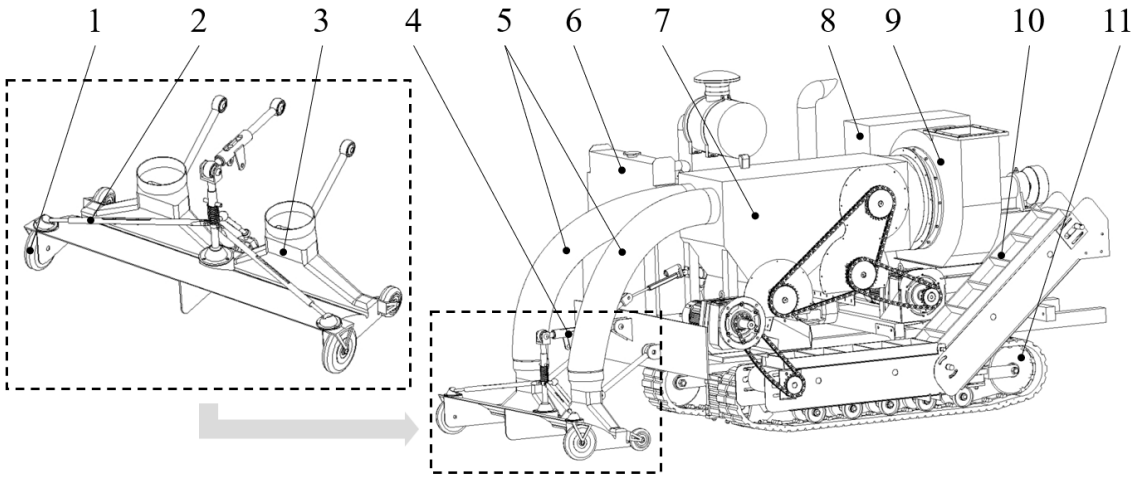

1. Copying wheel, 2. Follow copying mechanism, 3. Double air path pickup suction,
4. Suspension lifting parts, 5. Conveying hose, 6. Power system, 7. Cleaning separation device,
8. Control cabinet, 9. Centrifugal fan, 10. Conveyor, 11. Crawler-type walking chassis.
(a) Schematic diagram of prototype and device structure

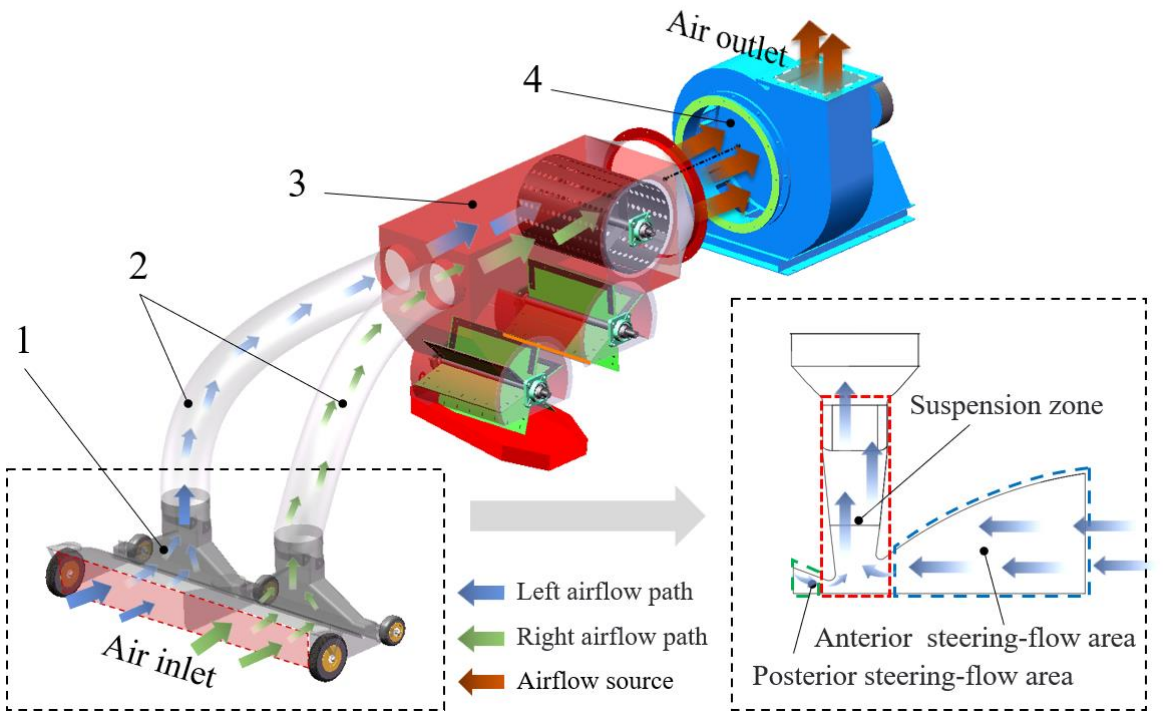

1. Dual-airway pickup suction port, 2. Conveying hose,
3. Cleaning separation device, 4. Centrifugal fan.
(b) Working principle

Figure 1. Structure diagram and schematic diagram.

flow area, return to the suspension area and ultimately enter the pneumatic conveying system propelled by the negative pressure airflow.

2.2. Determination of structural parameters of dual-airway pickup suction mouth

The team's preliminary experiment revealed that the structure of the picking up suction mouth has a significant impact on the flow field distribution throughout the entire pneumatic conveying system. A well-optimized flow field distribution can effectively enhance the working width and picking rate of fallen jujube fruit. Therefore, the design of the cavity structure of the picking up suction mouth holds paramount importance. As illustrated in Figure 2, the cavity structure parameters in this study encompass the suction inlet cross-section area S_A (by suction length L and suction width B), falloff angle α, shoulder height h, outlet diameter D, lead cavity length L, lead cavity section height H, flanging radius r, and the relative height of h_g.

2.2.1. Cross-sectional area of suction inlet

The suction inlet's cross-sectional area takes a rectangular shape, predominantly governed by two parameters: the length L and width B of the suction inlet. The length of the suction port L defines the working width of the device, and employing a parallel double suction port with L = 1400 mm guarantees suitable power and working width.

Once the airflow rate and suction length are determined, the average wind speed at the suction inlet section is affected by the suction width B. Its value must surpass the jujube suspension speed. The relationship between the average wind speed $\overline{V}$ of the intake cross section and the suction width B is as follows (1):

$$\bar{V} = \frac{Q}{7200\kappa(L+B)h_g} > V_f \ , \qquad (1)$$

where $\overline{V}$ is the average wind speed of the suction inlet cross section, m/s; Q represents the airflow picked up at the inlet of the suction port, m³/h; κ is the safety factor, typically ranging from 1.2 to 1.4; h_g is the relative height difference, m; V_f denotes the jujube suspension speed, m/s. In this paper, we examine the relationship between airflow (Q) and the parameters of the centrifugal fan in the test prototype. The airflow at the inlet of the pickup suction is determined to be 11,000 m³/h, with a safety factor (κ) of 1.3, suction length (L) of 1400mm, and a relative height difference (h_g) of 30 mm to ensure that the average wind speed surpasses the suspension speed of jujube.

The test results reveal that the maximum suspension velocity of jujube is 23.28 m/s. To accommodate the jujube particles, the width of the suction mouth should exceed the maximum diameter of both the transverse and vertical axes, leaving a sufficient margin. Setting B (suction mouth width) to be greater than or equal to 50 mm is recommended. By plugging these parameters into Equation (1), the average wind speed is calculated to be 26.47 m/s, and the acceptable range for the suction mouth width (B) is defined as $50 \le B \le 80$ mm.

2.2.2. Falloff angle

The velocity distribution of the flow field inside the suction nozzle is significantly correlated with the pressure loss due to the falloff angle α of the pickup suction nozzle (Jiang et al., 2022). Setting the falloff angle α of the suction shoulder to a right angle (90°) leads to a sharp change in the airflow direction through the suction shoulder, causing local energy loss and the formation of eddy currents within the internal flow field. When the falloff angle of the suction shoulder surpasses 150°, the difference between the average velocity of the shoulder and the center velocity at the outlet increases, resulting in uneven flow rates and

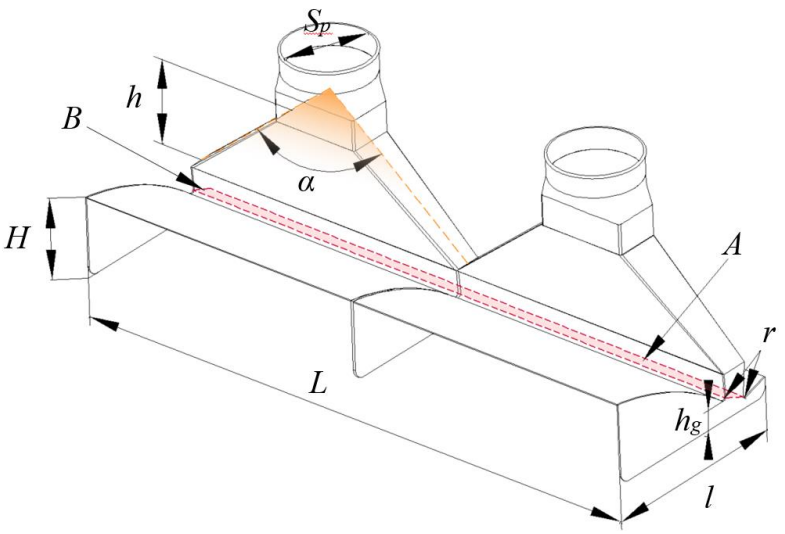

Figure 2. The structural parameters of the suction mouth.

elevated pressure loss. Therefore, the optimal range for the falloff angle α is between 90° and 150°.

2.2.3. Shoulder height

Shoulder height h is related to the spatial layout of the device, and is also related to the falloff angle and the length of the opening. Generally, to avoid interference of moving parts, the h value should not be too large. In our design, h = 200 mm is selected.

2.2.4. The diameter of the exhaust port

The exhaust port serves as a dual-airway for picking up the suction's negative pressure air outlet, connects to the conveying hose, and features a circular shape. When the flow rate is constant, the diameter of the exhaust port influences the velocity of the airflow into the pickup suction. The calculation formula for the diameter D of the exhaust port is presented in Equation (2):

$$D = \left[\frac{4Q}{3600\varphi V_f}\right]^{\frac{1}{2}}, \quad (2)$$

In the formula, Q represents the airflow at the suction entrance, m³/h; φ stands for the velocity coefficient, with a valid range between 1.3 and 10; V_f denotes the suspension speed of jujube, m/s; D signifies the diameter of the exhaust port, m.

In this study, the airflow at the suction inlet is set at 11,000 m³/h. The airflow path within the pickup suction mouth is straightforward, with a φ value of 1.3. The jujube suspension speed (V_f) is measured at 23.28 m/s. By inputting these parameters into Equation (2) and considering the dimensions of the cleaning device, the determined diameter of the exhaust port on both sides is 200 mm.

2.2.5. Length of the lead cavity

The lead cavity serves as the primary intake position of the suction mouth, and its length affects the initial speed of fallen jujube fruit transitioning from a static state to being picked up by the suction mouth. A smaller length results in a shorter duration for the jujube to be affected by the airflow, consequently reducing its movement speed. Conversely, a longer length accelerates the speed at which it reaches the pickup suction port. However, considering the operational gap between the suction port and the ground, an excessively long lead cavity leads to significant air dissipation along the cavity wall and the ground. This diminishes the air velocity within the lead cavity, which is not conducive to the movement of fallen jujube fruit after collection. Therefore, the designed lead cavity length l is set to 450 mm.

2.2.6. Section height of lead cavity

The section height of the lead cavity is related to the stacking height of fallen jujube fruit after stripping. In this paper, the section height of the lead cavity H is designed to be 180 mm, aligning with the conditions observed during the jujube orchard harvest period.

2.2.7. Flanging radius

The lead cavity is connected with the pickup suction port through a rolling edge with a specific curvature radius. The design of this rolling edge proves effective in minimizing local loss within the flow field. The size of the flanging radius r is pertinent to ensuring a smooth flow line in the internal flow field at the connection and managing the intensity of eddy currents. Its recommended value falls within the range of 0–15 mm.

2.2.8. The relative height difference

The relative height difference h_g signifies the vertical disparity between the front and back sides of the pickup suction. To ensure a smooth entry of jujube into the conveying air path system and minimize air dissipation at the suction section, the height of the front rolling edge above the ground should surpass the triaxial size of jujube. Conversely, the height of the back rolling edge above the ground must be less than the triaxial size of jujube. An appropriate relative height difference can provide the necessary pressure difference for jujube suspension, effectively reducing the dwell time of jujube in the cavity and enhancing pickup efficiency. The designed relative height difference is set within the range of 0–30 mm.

2.3. Construction of simulation system

2.3.1. Simulation model and grid division

An analysis of the flow field area was conducted on the dual-airway pneumatic fallen jujube fruit pickup device and its test prototype. The internal space, encompassing the dual-airway pneumatic conveying system, the pickup device, and the ground, was selected as the calculation area for simulation. A three-dimensional model of the dual-airway pickup suction mouth (depicted in Figure 3a) was created using SolidWorks. This model was then imported into ANSYS FLUENT to extract the fluid domain and generate the numerical model.

Treating the model as a completely closed entity, all narrow gaps were disregarded. In the Mesh module of ANSYS Workbench, the Adaptive function was employed for unstructured mesh division, implementing local mesh refinement for the left and right corners of the pickup suction to enhance calculation accuracy. Coarse mesh division was applied to the remaining fluid areas. The total number of meshes in the numerical simulation model amounted to approximately 495,000 and 297,000, respectively.

Upon smoothing the meshes, the Aspect Ratio of the meshes fell within the range of 0.2 to 1.0, Equivolume Skewness was less than 0.8, and the meshing results are displayed in Figure 3b.

2.3.2. Gas governing equation

The airflow within the pneumatic conveying system and the dual-airway pickup suction body was characterized as

steady viscous flow. Given the low flow velocity within the fluid domain of the numerical model, it could be treated as incompressible air, following the principles outlined by Klainerman and Majda (1982). Under these conditions, the gas flow state adhered to the mass conservation equation and the momentum conservation equation, as follows:

$$\frac{\partial \rho}{\partial t} + \frac{\partial}{\partial x_i}(\rho \mu_i) = s_m \,, \tag{3}$$

$$\frac{\partial}{\partial t}(\rho \mu_i) + \frac{\partial}{\partial x_i}(\rho \mu_i \mu_j) = -\frac{\partial p}{\partial x_i} + \frac{\partial \tau_{ij}}{\partial x_j} + \rho g_i + F_i \,, \tag{4}$$

where ρ is fluid density, kg/m^3; μ_i, μ_j is mean flow velocity component, m/s; p is static pressure, Pa; x_i, x_j is Cartesian coordinate system; τ_{ij} is stress tensor; g_i is the gravitational volume of the direction; F_i is external volume force, N.

The Standard Model is chosen for its elevated stability and computational accuracy, making it the preferred selection for numerical model simulation. The turbulent kinetic energy equation and the turbulent dissipation rate equation are solved, leading to a cumulative solution. Subsequently, the turbulent viscosity is calculated based on the obtained solution value. Finally, the Reynolds stress solution is derived through the Boussinesq hypothesis (Könözsy and Könözsy, 2019), and the governing equation is formulated as follows:

$$\frac{\partial(\rho k)}{\partial t} + \frac{\partial(\rho k u_i)}{\partial x_i} = \frac{\partial}{\partial x_j}\left[\left(\mu + \frac{\mu_t}{\sigma_k}\right)\frac{\partial k}{\partial x_j}\right] + G_b - \rho\varepsilon - Y_M + S_k \,, \tag{5}$$

$$\frac{\partial(\rho \varepsilon)}{\partial t} + \frac{\partial(\rho \varepsilon u_i)}{\partial x_i} = \frac{\partial}{\partial x_j}\left[\left(\mu + \frac{\mu_t}{\sigma_{2\varepsilon}}\right)\frac{\partial \varepsilon}{\partial x_j}\right] + G_{1\varepsilon}\frac{\varepsilon}{k}(G_k + G_{3\varepsilon}G_b) - C_{2\varepsilon}\rho\frac{\varepsilon}{k} + S_\varepsilon \,, \tag{6}$$

where G_k is the production term of turbulent kinetic energy k caused by the average velocity gradient; G_b is the production term of turbulent kinetic energy k caused by buoyancy; Y_M is pulsation expansion term in compressible turbulence; $C_{1\varepsilon}$, $C_{2\varepsilon}$, $C_{3\varepsilon}$ is empirical constant; σ_k, σ_ε is the Prandtl number corresponding to k and ε; S_k, S_ε is user-defined source entry.

In the standard k- ε model, according to the recommended value of Launder et al., and later experimental verification, $C_{1\varepsilon}$=1.44, $C_{2\varepsilon}$=1.92, $C_{3\varepsilon}$=0.09. σ_k =1.0 , σ_ε=1.3. For incompressible fluids, G_b =0, Y_M =0, S_k =0, S_ε=0.

2.3.3. Parameter setting of simulation system

In this paper, the fluid domain material in the suction mouth is air, the density is 1.205 kg/m^3, and the air viscosity is 1.85 × 10^{-5} Pa*s; inlet boundary conditions are used for the end face of the dual-airway exhaust port, outlet boundary conditions are used for the anterior and posterior steering-flow surfaces of the pickup suction port, and nonslip wall boundary conditions are used for the walls.

In accordance with the practical operation of the air path conveying system, the airspeed achievable by the centrifugal fan ranges from 0 to 45 m/s. The inlet is configured as a velocity outlet boundary condition. Due to the negative pressure conveying, the inlet wind speed at the exhaust port section is determined based on wind speed measurements at the end of the double-suction conveying hose of the test prototype. It is set as –40 m/s, and its direction is perpendicular to the inlet surface.

The outlet boundary is governed by the pressure outlet condition, with the atmospheric pressure set as the boundary value, aligning with the actual working conditions. The inlet turbulence parameters can be computed using the Reynolds number calculation formula and the turbulence intensity calculation formula.

2.3.4. Determination of simulation test factors

The inlet velocity of the suction port is closely related to the structural parameters that form the inlet section. A uniform velocity distribution in the inlet section is crucial, ensuring sufficient airflow velocity for the suspension of jujube particles. Based on the conclusions drawn in Section 2.2, certain structural parameters of the inlet have been designed and finalized.

To investigate the influence of undetermined cavity structural parameters within the dual-airway pickup inlet on the test index, a simulation experiment was designed. The experimental factors included falloff angle, suction width, flanging radius, and relative height difference, while the inhomogeneous coefficient of velocity served as the experimental index.

Referring to the summary in Section 2.2, the falloff angle (A) was set between 90° and 150°, suction width (B) was set between 50 and 80 mm, flanging radius (C) was set between 0 and 15 mm, and relative height difference (D) was set between 0 and 30 mm. The test factors and their corresponding horizontal coding table are detailed in Table 1.

2.3.5. Determination of simulation test indexes

The solution calculation method employs a pressure-based solver, steady-state flow, and the SIMPLE algorithm. Convergence is considered achieved when the residual accuracy is less than 10^{-3}. To articulate key numerical results regarding the airflow state in the pneumatic conveying system and pickup suction port, three sections—S_1, S_2, and S_3—were intercepted for distinct simulation analyses, as illustrated in Figure 3c. S_1 represents the vertical plane connecting the center of the cross-section of two exhaust ports. S_2 is the vertical plane perpendicular to the center of the exhaust port passing through the left suction port. S_3 is the oblique section plane that varies with the parameters of the suction inlet section.

Table 1. Experimental factors and levels.

Factors	Levels						
	1	2	3	4	5	6	7
A/ (°)	90	100	110	120	130	140	150
B/ m s^{-1}	50	55	60	65	70	75	80
C/ m s^{-1}	0	2.5	5	7.5	10	12.5	15
D/ m s^{-1}	0	5	10	15	20	25	30

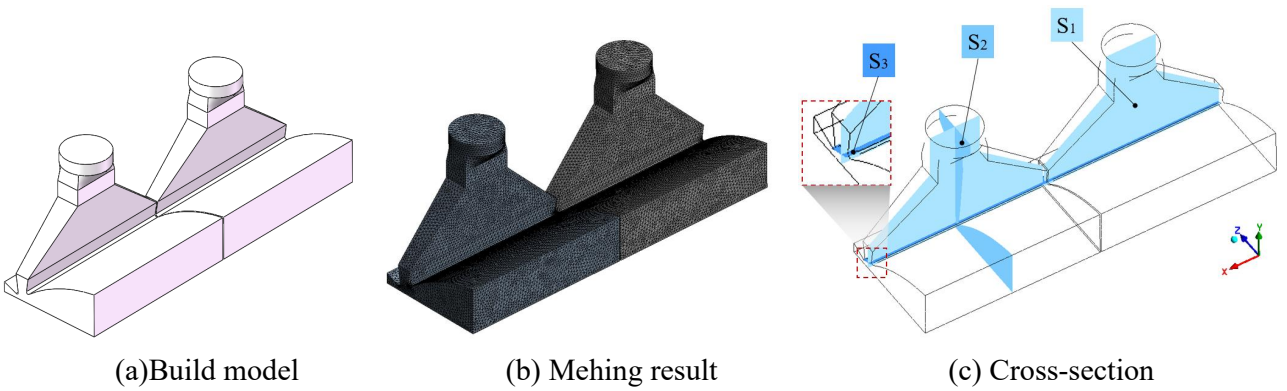

Figure 3. Meshing result and cross-section of values taken.

The inlet velocity is closely related to the structural parameters constituting the inlet cross-section. The velocity distribution in the inlet cross-section should be uniform, providing ample air velocity for the suspension of jujube particles. Consequently, the velocity unevenness coefficient (*M*) is selected as the evaluation index (Wang et al., 2019). A more uniform airflow distribution in the suction section is indicated by a lower *M*. The calculation method is expressed in Equation (7).

$$M = \frac{\sqrt{\frac{1}{n-1}\sum_{i=1}^{n}(V_i - \bar{V}_a)^2}}{\bar{V}_a} \times 100\%, \qquad (7)$$

where n is the number of measuring points; V_i is i line suction section airflow rate, m/s; $\overline{v_a}$ is the average air velocity at suction section, m/s.

2.4. Optimization and test of structural parameters of dual-airway pickup and suction mouth

In this study, the velocity unevenness coefficient was adopted as the test index, with the falloff angle, suction width, flange radius, and the relative height difference considered as test factors. A single-factor test was executed to determine the optimal value range for each factor. Additionally, a four-factor and three-level test scheme was designed using the Box-Behnken experimental design method in Design-Expert 11.0 software. Ultimately, the composite optimization function was employed to optimize the key structural parameters of the dual-airway pickup.

Simultaneously, to validate the accuracy of the constructed simulation model and the results of parameter optimization, a dual-airway pneumatic landing red date pickup device underwent trial production. The device was installed on a test prototype, and the optimized cavity structure parameters were tested and verified at the Engineering Training Center of Shihezi University in March 2022.

3. Results

3.1. Analysis of the influence of single factor test of each structural parameter on velocity uniformity

The preliminary experimental results from our research group indicate that the factors affecting the velocity uniformity of the inlet section in the dual-airway pickup inlet are primarily associated with four structural

parameters: cavity falloff angle, suction width, flanging radius, and relative height difference cell. Building on the summary conclusions in Section 2.2 and the summary factor levels in Section 2.3.4, the average velocity at the exhaust port section was determined to be –40 m/s.

To pinpoint the optimal value range for the structural parameters of the dual-airway pickup and suction mouth, including the addition of a central separator, a single-factor test was conducted. Section S1 was designated as the reference section, and 140 measuring points (70 for each left and right suction port) were evenly positioned along the intersection line between this section and the oblique section of the suction mouth. Subsequently, the data results were extracted and analyzed.

3.1.1. Influence of falloff angle on airflow velocity at suction section

Constrained by the working width of the dual-airway pickup outlet, the falloff angle (α) of the suction outlet varies from 90° to 150° with a 10° interval. Under the conditions where the suction outlet width is 50 mm, the relative height difference is 20 mm, and the flange radius is 7.5 mm, the measurement points at different falloff angles and the velocity curves of these measuring points are illustrated in Figure 4a. The measuring point with a velocity of 0 corresponds to the position of the middle partition board, and it was excluded from subsequent data processing.

The graph indicates that with an increase in the falloff angle of the dual-airway pickup mouthpiece, the velocity fluctuation in the mouthpiece section gradually intensifies, displaying a "double peak" trend. The peak velocity is observed near the middle cavity of the left and right mouthpieces, and the airflow velocity near the wall significantly diminishes.

Simultaneously, the relationship curve of velocity unevenness coefficient to falloff angle and average velocity in Figure 4b reveals a positive correlation between the velocity unevenness coefficient and the variation in falloff angle. It demonstrates an initial steady increase followed by a sharp rise. This trend is primarily attributed to the increasing falloff angle, causing a gradual decrease in the distance between the exhaust port section and the suction section. In other words, as the height of the suction shoulder decreases, the airflow velocity on both sides of the suction shoulder decreases significantly, leading to a substantial velocity difference along the length of the suction section, resulting in a "double peak" trend. The falloff angle has a minor impact on the average airflow velocity of the suction section, exhibiting minimal fluctuation. Consequently, the optimal value range for the falloff angle of the pickup suction is determined to be 90° to 110°.

3.1.2. Influence of suction width on airflow velocity of suction section

To determine the appropriate suction width and enhance the airflow velocity and negative pressure value in the suction section, the suction width (B) is varied from 50 to 80 mm with a 5 mm interval. Under the conditions where the falloff angle is 120°, the relative height difference is 20 mm, and the flanging radius is 7.5 mm, the measurement points for different suction widths and the velocity curves of these points are depicted in Figure 4c. The relationship between suction width, average velocity, and velocity unevenness coefficient was analyzed, and the corresponding relationship curve is presented in Figure 4d.

Analyzing Figure 4c and Figure 4d, it is observed that the velocity fluctuation at the measuring point in the suction mouth follows a similar pattern, with the peak velocity occurring in the middle of the left and right suction mouth body. The velocity unevenness coefficient exhibits a positive correlation with the numerical change in suction mouth width, increasing steadily at first, sharply increasing, and finally gradually increasing with the widening of the suction mouth.

Additionally, the average velocity shows a negative correlation with the numerical change in suction mouth width, implying that the average velocity decreases with an increase in the suction mouth width. This change is attributed to the fact that the cross-sectional area of the suction mouth is determined by its width. With the flow rate held constant, the increased cross-sectional area of the suction mouth leads to a reduction in airflow velocity through the suction mouth. To ensure that the suction cross-section can provide sufficient air velocity for jujube particle suspension, the optimal value interval for the suction width is determined to be 50 to 60 mm.

3.1.3. Influence of flanging radius on airflow velocity at suction section

The suction mouth body and the drainage plate are connected by a rolling arc, effectively smoothing the airflow and reducing eddy current loss inside the cavity. This rolling arc connection also minimizes damage to jujube particles during the picking process. Considering the structural dimensions of the suction, the flanging radius (r) is determined to range from 0 to 15 mm with a 2.5 mm interval. Under the conditions of a 100° falloff angle, a 55 mm suction width, and a 20 mm relative height difference, the curves of measuring points with different flanging radius and the velocity at these points are illustrated in Figure 4e.

The airflow velocity fluctuation of the suction section without the flanged arc connection is substantial, and the velocity fluctuation decreases significantly after the flanged arc connection. However, the velocity fluctuation gradually increases with the rise in the flanging radius. The fluctuation trend of the suction section with the flanged arc connection is smaller than that of the suction section without the flanged arc connection.

The relationship between the flanging radius, average velocity, and velocity unevenness coefficient is examined

in Figure 4f. The suction section without a flanging arc connection exhibits a large velocity unevenness coefficient and low average airflow velocity, attributed to significant eddy current loss caused by airflow through the connection. The velocity unevenness coefficient decreases significantly and then gradually increases with the growth of the flanging radius, while the average airflow velocity decreases with the increase in the flanging radius. To ensure better velocity distribution in the suction section and higher airflow velocity, the optimal range for the flanging radius is determined to be 5-10 mm.

3.1.4. Influence of relative height difference on airflow velocity at suction section

The anteri-or and posterior steering-flow plates are connected to the suction port, and the connection between the centers of the front and back of the rolling edge determines the width of the suction port. The difference in height from the ground is also a key parameter affecting the suction port section. While fully considering the structural size of the suction, it is determined that the relative height difference (h_g) ranges from 0 to 30 mm with an interval of 5 mm. Under the conditions of a 110° falloff angle, a 50 mm suction width, and a 7.5 mm flanging radius, the curves of different relative height differences and the velocity at measuring points are depicted in Figure 4g.

Analyzing Figure 4g, with the gradual increase in the relative height difference, the "double peak" trend formed by velocity fluctuation gradually becomes flatter, and the fluctuation range significantly decreases. Figure 4h indicates that the velocity unevenness coefficient decreases with the increase in the relative height difference. However, when the relative height difference exceeds 25 mm, the velocity unevenness coefficient shows an increasing trend. Conversely, with the increase in relative height difference, the average velocity exhibits a slow increase at first, then maintains a steady state, and finally declines sharply. Therefore, the optimal value range for the relative height difference, to maintain a low velocity unevenness coefficient and a high average velocity, is determined to be 15–25 mm.

3.2. Orthogonal test

Based on the results of single factor test, the optimal ranges of falloff angle, suction width, flanging radius, and relative height difference are determined to be 90°–110°, 50–60 mm, 5–10 mm, and 15–25 mm, respectively. Following the test method outlined in Section 2.3, the velocity unevenness coefficient is calculated in combination with Equation (7). The test scheme and test results are shown in Table 2.

The analysis of the velocity unevenness coefficient for the airflow rate at the suction section of the dual-airway is conducted through regression. The quadrivariate regression model for the velocity unevenness coefficient for each factor is obtained, as Equation (8) shows:

$$Y_c = 103.02325 - 1.96797A + 1.09951B - 2.58340C - 3.10571D + 0.01360AB + 0.01528AC - 2.61223 \times 10^{-3}AC - 0.05646BC - 0.01793BD + 0.07027CD + 0.01424A^2 + 3.48494 \times 10^{-3}B^2 + 0.20173C^2 + 0.04752D^2 \quad (8)$$

ANOVA was conducted based on the velocity unevenness coefficient regression model outlined in Table 3. The p-value for the established regression model was found to be <0.0001, while the p-value for the missing item was calculated as 0.1295, exceeding the 0.05 threshold. These results suggest a significant effect of the model. The coefficient of determination $R^2 = 0.9627$ indicates that the misfit of the response value analyzed by this model only accounts for 3.73% of the total. The correction determination coefficient Adj $R^2 = 0.9255$ also shows a significant effect of the model. Among them, A, B, A^2, C^2, and D^2 exhibited significant effects on velocity unevenness coefficient ($p < 0.01$), while AB, BC, and CD demonstrated significant effects on the velocity unevenness coefficient at a slightly lower significance level ($p < 0.05$).

In order to directly describe the influence of interaction among falloff angle, suction width, flanging radius, and relative elevation on the coefficient of velocity unevenness, the response surface plot and contour plot were drawn by Design-Export 11.0 test Design software, where any two factors varied within the range of optimization level, while the other two factors remained unchanged at the intermediate level (Figure 5).

Figure 5a reveals that, with constant flanging radius and relative height difference, the velocity unevenness coefficient exhibits a slow increase as the suction width increases. It demonstrates a pattern of gradual change initially, followed by a gradual increase with the rise of the contraction angle over time. Additionally, the contour plot in Figure 5a illustrates that the change rate of the velocity unevenness coefficient concerning the direction of falloff angle is higher compared to the direction of suction width. In other words, the influence of the falloff angle on the velocity unevenness coefficient is greater than that of other factors.

In Figure 5b, with a constant suction mouth width, the velocity unevenness coefficient exhibits a trend of initially decreasing slowly and then gradually increasing with the increase of the flanging radius. Conversely, when the flanging radius is constant, the velocity unevenness coefficient is positively correlated with the suction mouth width, increasing with the increase of the suction mouthwidth. This phenomenon is attributed to the significant role played by the suction flanging structure in smoothing the airflow. An excessively small flanging radius can lead to energy dissipation and abrupt velocity changes in the flow, while an overly large flanging radius can decrease the average airflow velocity at the suction cross-section, resulting in an increased velocity unevenness coefficient. Simultaneously, the increased cross-sectional area of the suction port, with no change

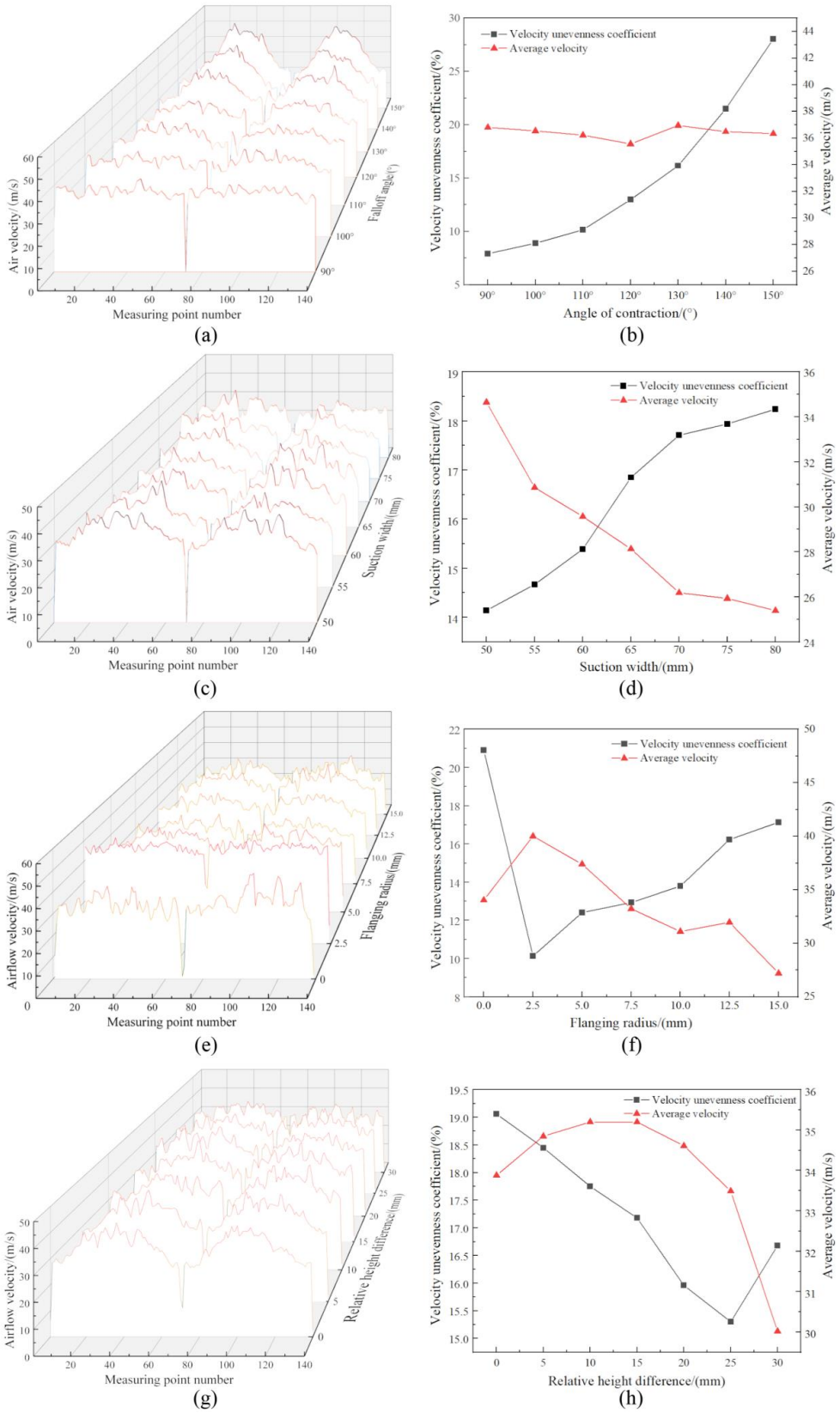

Figure 4. Effect of each single factor on the airflow velocity.

Table 2. Test scheme and results.

Test number	Experimental factors				Response indicators
	Falloff angle A/°	Suction width *B*/mm	Flanging radius *C*/mm	Relative height difference *D*/mm	Velocity unevenness coefficient *Y*/%
1	100	50	10	20	8.9
2	90	50	7.5	20	5.89
3	100	55	10	15	8.75
4	100	50	7.5	25	7.52
5	90	60	7.5	20	6.95
6	110	60	7.5	20	9.88
7	100	55	7.5	20	6.45
8	100	60	7.5	15	7.95
9	100	60	7.5	25	9.20
10	100	55	7.5	20	7.54
11	100	55	7.5	20	6.79
12	110	55	7.5	25	11.38
13	100	55	5	25	8.27
14	100	50	7.5	15	7.94
15	90	55	7.5	15	7.11
16	110	55	7.5	15	10.97
17	100	55	7.5	20	6.73
18	100	60	5	20	8.55
19	90	55	10	20	8.14
20	100	60	10	20	8.67
21	90	55	7.5	25	7.78
22	100	55	5	15	9.83
23	90	55	5	20	7.33
24	100	50	5	17.5	6.80
25	100	55	7.5	17.5	6.90
26	110	50	7.5	17.5	12.01
27	100	55	10	20	8.97
28	110	55	10	17.5	12.31
29	110	55	5	17.5	10.85

Table 3. Velocity unevenness coefficient regression model variance analysis.

Source	Quadratic sum	DOF	MSE	F value	p-value	Significance
Model	79.73	14	5.69	25.83	<0.0001	**
A	33.7	1	33.7	152.85	<0.0001	**
B	0.032	1	0.032	0.14	0.7094	-
C	0.49	1	0.49	2.24	0.1566	-
D	3.42	1	3.42	15.51	0.0015	**
AB	1.78	1	1.78	8.08	0.013	*
AC	0.53	1	0.53	2.4	0.1433	-
AD	0.072	1	0.072	0.33	0.5761	-
BC	1.9	1	1.9	8.62	0.0108	*
BD	0.83	1	0.83	3.77	0.0725	-
CD	1.9	1	1.9	8.62	0.0108	*
A^2	13.1	1	13.1	59.41	<0.0001	**
B^2	0.049	1	0.049	0.22	0.6462	-
C^2	9.78	1	9.78	44.34	<0.0001	**
D^2	7.25	1	7.25	32.89	<0.0001	**
Residual	3.09	14	0.22			
Lack of fit	2.44	11	0.22	1.02	0.5628	not significant
Error	0.65	3	0.22			
SUM	82.82	28				

R^2-0.9627, Adj R^2-0.9255, Pred R^2-0.8013
**p < 0.01 was very significant, *p < 0.05 was significant.

in flow rate per unit time, leads to decreased airflow velocity at the shoulder position near the falloff angle on both sides, causing uneven airflow velocity distribution and an elevated velocity unevenness coefficient. In Figure 5c, the response surface diagram depicts the interaction between flanging radius and relative height difference on the velocity unevenness coefficient. It indicates that, with a constant flanging radius, the relative height difference is negatively correlated with the velocity unevenness coefficient and has minimal impact on this index. On the other hand, with a constant relative height difference, the velocity unevenness coefficient initially decreases and then gradually increases with the growth of the relative height difference. The contour map illustrates that the velocity unevenness coefficient experiences a more pronounced change with the relative height difference than the flanging radius. In essence, the influence of the relative height difference on the velocity unevenness coefficient surpasses that of the flanging radius.

3.3. Parameter optimization and verification

3.3.1. Parameter optimization

To optimize the structural parameters of the dual-airway pickup outlet, the Optimization module was employed to optimize the regression model. Among the test factors, the falloff angle ranged from 90° to 110°, the suction width from 50 to 60 mm, the flanging radius from 5 to 10 mm, and the relative height from 15 to 25 mm. The minimum

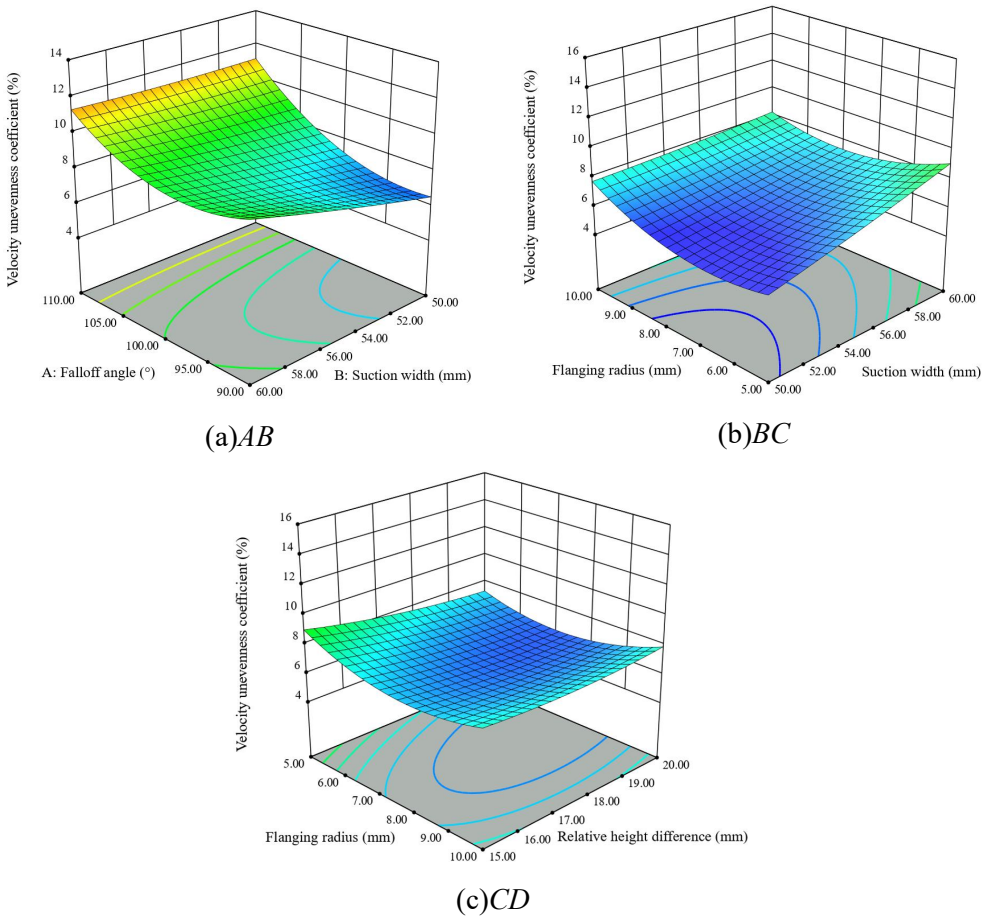

Figure 5. Effect of test factors on velocity unevenness coefficient.

value of the velocity unevenness coefficient of the test index is selected, and the objective function and constraint conditions are established:

$$\begin{cases} minY(A,B,C,D) \\ s.t. \begin{cases} -1 \le A \le 1 \\ -1 \le B \le 1 \\ -1 \le C \le 1 \\ -1 \le D \le 1 \end{cases} \end{cases}$$

The optimal combination is obtained as follows: the falloff angle is 91.37°, the opening width is 50 mm, the flanging radius is 6.45 mm, and the relative height is 20 mm. In this case, the velocity unevenness coefficient is 5.89%.

3.3.2. Test verification

To validate the accuracy of the numerical simulation for the dual-airway pickup suction, a physical device incorporating the optimal parameter combination was fabricated and tested at the Engineering Training Center of the School of Mechanical and Electrical Engineering, Shihezi University. The test setup included a test prototype equipped with an 11 kW centrifugal fan, a Delta MS300 inverter, a dual-airway pneumatic fallen jujube fruit pickup device, and an SYT-2000V intelligent digital pressure anemometer, as depicted in Figure 6.

Upon starting the prototype, the frequency converter in the control cabinet was adjusted to vary the centrifugal fan's speed, stabilizing the wind speed at the exhaust section to a measured value of 40 m/s. Subsequently, 70 measurement points were uniformly selected in the middle position of the dual-airway suction section, and wind speed was measured. Each measurement point was maintained for 3 s, and the data were recorded and measured three times to obtain the average value as the final measurement result. Finally, the measured air velocity results of the suction section were compared with the numerical simulation results.

Upon analyzing the test data, it was observed that the velocity distribution at the measuring points closely resembled the simulation results. Some differences in airflow velocity were noted at specific measuring points,

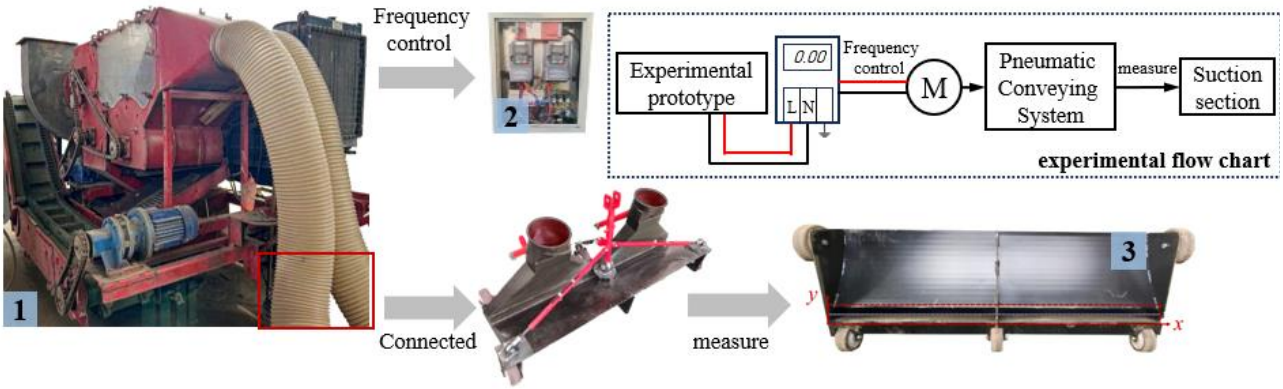

1. Test prototype, 2. Frequency converter regulation,
3. Dual-airway pickup suction port, and section to be measured.

Figure 6. Experimental device diagram.

primarily in the area directly under the dual-airway pickup's suction outlet, where the airflow velocity displayed significant fluctuations. However, the simulated velocity at the suction cross section exhibited a generally consistent distribution trend with the measured values. The velocity unevenness coefficient for the three test values was 6.22%, 6.60%, and 6.45%, respectively. The maximum deviation from the optimized simulation value was 0.71%, and the maximum relative error was 12.05%. The test results aligned well with the simulation outcomes, suggesting that the model design optimization is reasonable. It can effectively simulate the changes and distribution of wind speed in the suction mouth, positively impacting the velocity uniformity of the flow field in the dual-airway suction mouth.

4. Discussion

The existing prototype for jujube harvesting primarily performed the jujube pickup operation using a single gas path arrangement and manual handling with straws. This approach encountered challenges such as a limited sweep operation area for a single pickup and the necessity for manual assistance. A notable correlation was identified between the dust suction effect and the suction port's structure. While this suction port cannot be directly compared with the dual-airway pickup suction port in this paper due to different scenarios and objects, its research methodology holds significant guiding significance for this study. Furthermore, existing research on agricultural material pickup suction structures has only conducted qualitative analyses on the suction characteristics' shape, lacking an in-depth exploration of the suction structure.

To design an effective pickup suction that broadens the pickup area and enhances the one-time pickup capacity, we delved into the key structural parameters of the dual-airway pickup suction body using computational fluid dynamics. This method, in comparison to traditional structural parameter design, boasts advantages such as environmental friendliness, cost-effectiveness, and a shorter design cycle. Numerical simulation revealed that the dual-airway pickup nozzle design is more conducive to jujube particle pickup and migration, ultimately improving suction nozzle performance. Single-factor tests on falloff angle, suction width, flanging radius, and relative elevation, which affect the airflow velocity at the suction cross-section, showed that falloff angle and suction width significantly influence the velocity unevenness coefficient, exhibiting a noticeable trend with increasing experimental factors. The flanging radius significantly affects airflow smoothing and turbulence reduction in the pickup mouth.

After optimizing the structural parameters, the velocity unevenness coefficient of air flow at dual-airway pickup mouth section decreases significantly. The main reasons for this are as follows: first, the shrinking angle has a great influence on the velocity uniformity of the duckbill type flat long mouth. The selection of the appropriate shrinking angle within the effective parameter range greatly reduces velocity fluctuation and results in a more uniform distribution of air velocity. Second, a smooth transition is adopted at the suction section to avoid abrupt airflow velocity and reduce turbulent dissipation, so the velocity unevenness coefficient is significantly reduced. Thirdly, the relative height difference causes the suction section to tilt to different degrees, and the air intake angle from the front lead cavity decreases while the air intake

Angle from the rear lead cavity increases. As a result, the velocity unevenness coefficient gradually decreases with the increase of the relative height difference. Therefore, the velocity unevenness coefficient effectively decreases. Since the suction width determines the suction section area, thus affecting the air intake, under the condition of constant flow, the cross-section area decreases or increases, and the airflow velocity through the cross-section increases. In order to improve the working efficiency of the suction section with a larger average airflow velocity, a smaller suction width is selected in this paper.

From the analysis of the verification test results, it can be seen that the test results are basically consistent with the numerical simulation results. There is a small amount of error between the optimized dual-airway pickup suction and the numerical simulation results. The main reason for this is that in the verification test, in order to facilitate the measurement, the number of selected measurement points is only half of the number of numerical simulation measurement points. The data accuracy is insufficient compared with the simulation results, but the error is within the acceptable range.

The dual-airway pneumatic fallen jujube fruit pickup device designed in this paper increases the working width by adjusting the suction cross-section area, and conducts numerical simulation and optimization on the suction structure parameters by determining the key structural parameters affecting the velocity heterogeneity of the suction cross section, and finally obtains the best suction body structure parameters. This research holds significant importance for the optimization of complex cavity structures in pickup equipment design, offering a novel idea and method for the development of red date pickup equipment. With its advantages of low cost and a short design optimization period, this research method is expected to make new breakthroughs in the application of red jujube pickup equipment.

5. Conclusion

To address the challenge of the existing air-suction red date pickup machine not achieving mechanized pickup, this paper introduces the design of a dual-airway pneumatic fallen jujube fruit pickup device. Initially, a numerical simulation model of the flow field within the dual-airway pickup mouth, a pivotal component of the dual-airway pickup mouth, is constructed based on computational fluid dynamics method. The impact of the central separator on the cavity's flow field characteristics is thoroughly analyzed. Subsequently, employing the velocity unevenness coefficient as the response index, a single-factor test is conducted on key cavity structure parameters to identify the optimal value interval for each factor.

Through an orthogonal test, response surface analysis, and a composite optimization method, the optimal structural parameter combination is determined as follows: a falloff angle of 91.37°, an opening width of 50 mm, a flanging radius of 6.45 mm, and a relative height of 20 mm. Under these conditions, the velocity unevenness coefficient is measured at 5.89%. Validation tests under the optimal parameter combination conditions exhibit velocity unevenness coefficients of 6.22%, 6.60%, and 6.45%, respectively. The maximum deviation from the predicted value is 0.71%, and the maximum relative error is 12.05%.

Furthermore, the subsequent research in this paper will establish a CFD-DEM coupling simulation system, integrating the flow field of the pickup device and the dynamics of jujube particles. The paper aims to process and trial produce a dual-airway pneumatic landing jujube pickup prototype. Field experiments will be conducted to explore the movement characteristics of jujube in the dual-airway negative pressure pneumatic conveying system. This research will optimize the operating parameters of the device and ultimately determine the optimal working parameter combination for the device.

Acknowledgments

This research received support from the National Natural Science Foundation of China under grant numbers 52265038 and 52165037.

References

Blazek, J (2015). Computational fluid dynamics: principles and applications, Butterworth-Heinemann.

Dai JW, Xiao HW, Bai JW, Zhang Q, Xie L et al. (2013). Numerical simulation and optimum design on airflow distribution chamber of air-impingement jet dryer. Transactions of the Chinese Society of Agricultural Engineering 29 (3): 69-76.

Fu W, Zhang ZY, Ding K, Cao WB, Kan Z, Pan JB et al. (2018). Design and test of 4ZZ-4A2 full-hydraulic self-propelled jujube harvester. International Journal of Agricultural and Biological Engineering 11 (4): 104-110. http://doi.org/10.25165/j.ijabe.20181104.3981

Shi GK, Li JB, Ding LP, Kan Z (2022). Design and experiment of inertia pneumatic type cleaner system of jujube fruit. Nongye Jixie Xuebao/Transactions of the Chinese Society of Agricultural Machinery 53 (6).

He JY, Wen JB, Xiao S, Yang JC (2023). Multi-AUV Inspection for Process Monitoring of Underwater Oil Transportation. IEEE/CAA Journal of Automatica Sinica 10 (3): 828-830. https://doi.org/10.1109/JAS.2023.123117

Yang JC, Cheng C, Xiao S, Lan GP, Wen JB (2023). High Fidelity Face-Swapping With Style ConvTransformer and Latent Space Selection. IEEE Transactions on Multimedia: 1-12. https://doi.org/10.1109/TMM.2023.3313256

Jiang SQ, He ZH, Zhou YP, Xiao XW, Cao GD et al. (2022). Numerical simulation research on suction process of concrete pumping system based on CFD method. Powder Technology 409: 117787. https://doi.org/10.1016/j.powtec.2022.117787

Klainerman S, Majda A (1982). Compressible and incompressible fluids. Communications in Pure Applied Mathematics 35: 629-651. https://doi.org/ 10.1002/cpa.3160350503

Könözsy L, Könözsy L (2019). A New Hypothesis on the Anisotropic Reynolds Stress Tensor. A New Hypothesis on the Anisotropic Reynolds Stress Tensor for Turbulent Flows: Volume I: Theoretical Background and Development of an Anisotropic Hybrid k-omega Shear-Stress Transport/Stochastic Turbulence Model. Cham, Springer International Publishing: 105-135. https://doi.org/ 10.1007/978-3-030-13543-0_5

Li C, Deng YD, Xin YH (2016). Flow Field Analysis and Structure Optimization of the Suction Nozzle for Road Sweeper. SAE International. https://doi.org/10.4271/ 2016-01-1356

Li Y, Yang JC, Zhou Z, Wen JB, Kumar P (2022). Healthcare data quality assessment for cybersecurity intelligence. IEEE Transactions on Industrial Informatics 19 (1): 841-848. https://doi.org/10.1109/TII.2022.3190405

Li Y, Ercisli S (2023). Data-efficient crop pest recognition based on KNN distance entropy. Sustainable Computing: Informatics and Systems 38: 100860. https://doi.org/ 10.1016/j.suscom.2023.100860

Li Y, Ercisli S (2023). Explainable human-in-the-loop healthcare image information quality assessment and selection. CAAI Transactions on Intelligence Technology. https://doi.org/10.1049/cit2.12253

Li Y, Chao XW (2021). Toward Sustainability: Trade-Off Between Data Quality and Quantity in Crop Pest Recognition. Frontiers in plant science 12: 811241. https://doi.org/10.3389/fpls.2021.811241

Li Y, Chao XW (2022). Distance-entropy: an effective indicator for selecting informative data. Frontiers in Plant Science 12: 818895. https://doi.org/10.3389/fpls.2021. 818895

Li Y, Chao XW, Ercisli S (2022). Disturbed-entropy: A simple data quality assessment approach. ICT Express 8 (3): 309-312. https://doi.org/10.1016/j.icte.2022.01.006

Liu YX, Sang YY, Guo JY, Zhang TY, Wang H et al. (2021). Analysis of volatility characteristics of five jujube varieties in Xinjiang Province, China, by HS-SPME-GC/MS and E-nose. Food Science & Nutrition 9 (12): 6617-6626. https://doi.org/10.1002/fsn3.2607

Ni HJ, Zhang JQ, Zhao NS, Wang CS, Lv SS et al. (2019). Design on the winter jujubes harvesting and sorting device. Applied Sciences 9 (24): 5546. https://doi.org/10.3390/app9245546

Nie J, Jiang JC, Li Y, Wang HT, Ercisli S et al. (2023). Data and domain knowledge dual-driven artificial intelligence: Survey, applications, and challenges. Expert Systems: e13425. https://doi.org/10.1111/exsy.13425

Nie J, Wang Y, Li Y, Chao XW (2022). Artificial intelligence and digital twins in sustainable agriculture and forestry: a survey. Turkish Journal of Agriculture and Forestry 46 (5): 642-661. https://doi.org/10.55730/1300-011X.3033

Nie J, Wang Y, Li Y, Chao XW (2022). Sustainable computing in smart agriculture: survey and challenges. Turkish Journal of Agriculture and Forestry 46 (4): 550-566. https://doi.org/10.55730/1300-011X.3025

Olatunde G, Atungulu GG, Sadaka S (2016). CFD modeling of air flow distribution in rice bin storage system with different grain mass configurations. biosystems engineering 151: 286-297. https://doi.org/10.1016/j.biosystemseng.2016.09.007

Shi GK, Li JB, Kan Z, Ding LP, Ding HZ et al. (2022). Design and parameters optimization of a provoke-suction type harvester for ground jujube fruit. Agriculture 12 (3): 409. https://doi.org/10.3390/agriculture12030409

Wang XY, Shen L, Liu TT, Wei WW, Zhang S et al. (2022). Microclimate, yield, and income of a jujube–cotton agroforestry system in Xinjiang, China. Industrial Crops and Products 182: 114941. https://doi.org/10.1016/j.indcrop.2022.114941

Wang Y, Quan MF, Zhou Y (2019). Effect of velocity non-uniformity of supply air on the mixing characteristics of push-pull ventilation systems. Energy 187: 115962. https://doi.org/10.1016/j.energy.2019.115962

Xi Y, Zhang YL, Zhang XL, Dai Y (2020). Enhancement of particle collection efficiency considering the structural interplay: Particle motion characteristics analysis. Mechanics & Industry 21 (6): 618. https://doi.org/10.1051/meca/2020093

Xu HZ, Hua Y, He J, Chen QL (2022). The Positive and Negative Synergistic Airflow-Type Jujube Fruit Harvester (PN JH). Processes 10 (8): 1486. https://doi.org/10.3390/pr10081486

Yan M, Wang Y, Watharkar RB, Pu YF, Wu CY et al. (2022). Physicochemical and antioxidant activity of fruit harvested from eight jujube (Ziziphus jujuba Mill.) cultivars at different development stages. Scientific Reports 12 (1): 2272. https://doi.org/10.1038/s41598-022-06313-5

Yang JC, Zhang Z, Xiao S, Ma Sk, Li Y et al. (2023). Efficient data-driven behavior identification based on vision transformers for human activity understanding. Neurocomputing 530: 104-115. https://doi.org/10.1016/j.neucom.2023.01.067

Yang Y, Li Y, Yang JC, Wen JB (2022). Dissimilarity-based active learning for embedded weed identification. Turkish Journal of Agriculture and Forestry 46 (3): 390-401. https://doi.org/10.55730/1300-011X.3011

Ye J, Pan JB, Ai HJ, Wang JM (2022). Pure electric sweeper performance analysis and test verification of dust extraction port. Applied sciences 12 (10): 5188. https://doi.org/10.3390/app12105188

Zhang YC, Yang CZ, Baker C, Chen M, Zou X et al. (2014). Effects of expanding zone parameters of vacuum dust suction mouth on flow simulation results. Journal of Central South University 21 (6): 2547-2552. https://doi.org/10.1007/s11771-014-2210-2

Zhang ZY, Shi GK, Li JB, Wang XF, Ding LP et al. (2023). Analysis of jujube movement characteristics under positive and negative pressure airflow based on CFD-DEM. Computers and Electronics in Agriculture 210: 107902. https://doi.org/10.1016/ j.compag.2023.107902

Zhou J, Xu LY, Xuan Y, Xu YH, Liu GH (2020). Shedding frequency and motion of jujube fruits in various excitation modes. Transactions of the ASABE 63 (4): 881-889. https://doi.org/10.13031/trans.13776

Zhou L, Li JB, Ding LP, Ding HZ, Liang JP (2022). Analysis and Design of Operating Parameters of Floor-Standing Jujube Pickup Device Based on Discrete Element Method. Agriculture 12 (11): 1904. https://doi.org/10.3390/agriculture12111904

Zhou L, Li JB, Ding LP, Ding HZ, Shi GK et al. (2022). Design and evaluation of a mechanical floor-standing jujube picker. Agriculture 12 (8): 1203. https://doi.org/ 10.3390/agriculture12081203